Coastal Upwelling Viewed as a Stochastic Phenomenon

J. A. CARTON[1] AND S. G. H. PHILANDER

Geophysical Fluid Dynamics Program, Princeton University, Princeton, NJ 08540

(Manuscript received 20 December 1983, in final form 11 June 1984)

ABSTRACT

Four years of winds from the northeastern Pacific are used to drive a reduced-gravity ocean model which includes a high-resolution eastern coastal zone that spans 17° longitude and 30° latitude. Spectra of the alongshore velocity and interface height, measured in the coastal zone, are red to 100-day periods. At periods less than 50 days, 1) the circulation is strongly trapped within a radius of deformation of the coast and 2) the alongshore current is well correlated with the alongshore wind stress. At periods longer than 50 days, wind-stress curl becomes important. The alongshore pressure gradient becomes well correlated with the alongshore wind stress. Much of the ocean variability is at periods longer than 10 days. At periods longer than 100 days the alongshore currents begin to weaken and disperse away from the eastern boundary in a series of jets alternating northward and southward.

1. Introduction

In most studies of time dependent coastal upwelling the winds vary in an idealized manner. Charney (1955), Yoshida (1955), Allen (1976) and Suginohara (1982) assume that alongshore winds suddenly start to blow at time $t = 0$ and then remain constant. Philander and Yoon (1982) consider periodic winds. Carton (1984) describes the coastal response to an isolated storm. Realistic coastal winds are an essentially random succession of storms with differing scales. It is therefore appropriate to treat coastal upwelling as a stochastic process and to describe the oceanic response in a statistical rather than a deterministic manner. This paper provides such a description in terms of the mean and rms fields, spectra and cross-spectra between atmospheric and oceanic variables.

In order to study the forced response of a coastal ocean to realistic winds, we use actual winds from the eastern North Pacific for the period from January 1973 to November 1976 (part of a data set discussed by Willebrand, 1978). The statistics of the wind field are reviewed in Section 2. The analytical reduced-gravity model of Section 3 assumes that the winds are periodic in the alongshore direction. The numerical reduced-gravity model of Section 4 relaxes this assumption and is forced with the realistic winds. Time integrated statistics, spectra, and coherences are examined. The meridional component of the wind contains a strong seasonal cycle so the seasonal response is also considered.

[1] Present affiliation: Center for Earth and Planetary Physics, Harvard University, Cambridge, MA 02138.

2. Wind field

Surface pressure fields were obtained from the National Meteorological Center for the period January 1973 to November 1976. These data are available every 12 hours at 0000 and 1200 GMT. We analyze these data using the procedure of Willebrand (1978). First we compute geostrophic winds from the pressure field on a 1° × 1° grid. We make a 15° correction in direction and a 30% reduction in speed in order to account for surface frictional effects (consistent with Bakun's 1975 analyses). Wind stress is then computed from the geostrophic winds using a nonlinear bulk stress law. Comparing his computed winds with direct wind measurements, Willebrand found the error of all of these approximations to be less serious than the effects of deriving the wind field from smoothed pressure fields. The smoothing implicit in the pressure fields eliminates much of the wind variability with scales less than 1000 km. The smoothing strongly affects the wind-stress curl and might reduce the curl by as much as 50%. The four-year mean has been subtracted from the wind-stress data because this study only concerns the response to variable winds.

The rms zonal and meridional wind stress and wind-stress curl are displayed in Fig. 1. The meridional wind is strongest at 45°N and weakens towards the coast. The 20-year wind data set discussed by Nelson (1977) and Hickey (1979) shows a similar decay nearshore. The wind-stress curl is strongly concentrated at high latitudes.

Figure 2 shows an alongshore-versus-time cross section of low-pass filtered meridional wind stress (τ^y). The filter used here is a symmetric cosine filter

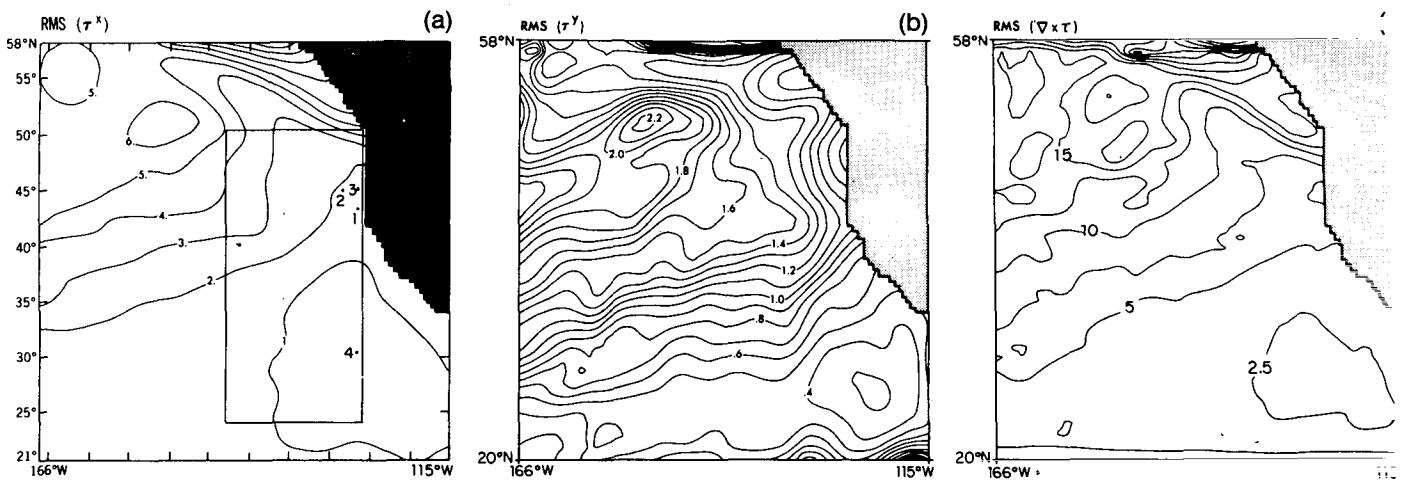

FIG. 1. Maps of the variability of the wind stress in the eastern North Pacific. The wind stress fields were deduced from NMC pressure analyses, using a procedure discussed in the text. (a) Root-mean-square (rms) zonal wind stress. Four years of twice-daily wind fields have been used in this computation. The rectangle marks the numerical model domain. Data from stations marked 1–4 are used in the time series analysis. (b) rms meridional wind stress. A nearshore maximum occurs at 45°N. The winds are generally stronger to the west. (c) rms $\nabla_h \times \tau * \nabla_h \times \tau$ increases poleward. Contour intervals are 1.0 dyn cm^{-2} and 2.5 × 10^{-8} dyn cm^{-3}.

with a total length of 150 days and a band width (as defined by Bloomfield, 1976, p. 202) of 110 days. The winds have a strong seasonal cycle above 30°N, northward in the winter and southward in the summer. A similar pattern was observed by Nelson (1977). The seasonal cycle in our data is fairly steady for 1973–75, but in the winter of 1975–76 the highest amplitude shifts northward.

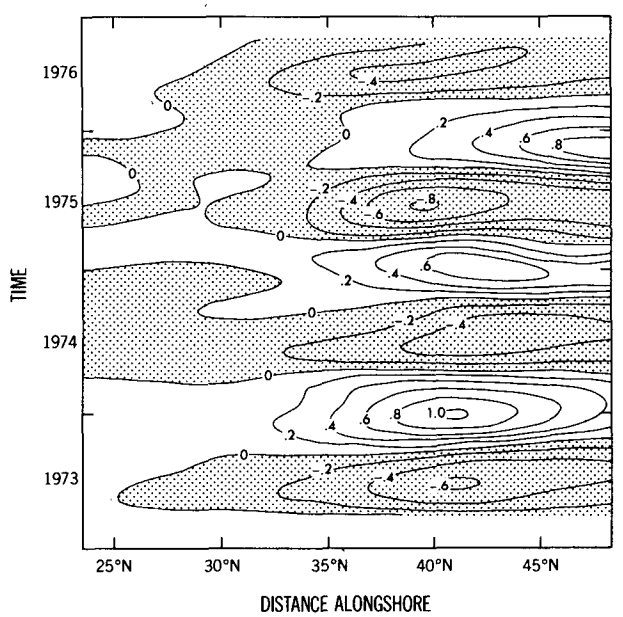

FIG. 2. Alongshore vs time cross section of low-pass filtered τ^y at 125°W. The low-pass filter has a bandwidth of 110 days. Data have been lost from the beginning and end of the record because of filtering. The contour interval is 0.2 dyn cm^{-2}. Shaded regions are negative.

Power density spectra of τ^y from 30 and 45°N (stations 3 and 4) are shown in Fig. 3. The spectra have been computed by cutting the time series into seven overlapping 350 day records. The mean and trend for each record were removed and the records were treated with a Hanning window. The resulting spectra were combined and frequency-averaged. The spectra are generally white for periods greater than 10 days, with stronger winds and an indication of the seasonal cycle at 45°N. Spectra obtained by combining the winds from three summers (1 April through 3 September), and also three winters (1 October through 31 March) are displayed in the same figure. Winter winds are generally stronger than summer winds and contain more energy at high frequencies, associated with winter storms.

Alongshore coherence of the meridional stress, shown in Fig. 4, has been computed between a point nearshore at 45°N (station 3, Fig. 2) and a point 880 km to the south by breaking the original time series into overlapping six month segments. The coherence is noisy but indicates that the spatial scale of the meridional stress increases with increasing period for periods less than 10 days. Taking the distance over which the wind is correlated with a coherence of 0.5 as a measure of the scale of the wind, at periods greater than 10 days this scale is ~1000 km. There is an indication of a small alongshore phase difference with the wind at high latitude lagging behind the wind at lower latitude. In general these results are consistent with observations summarized by Hickey (1979).

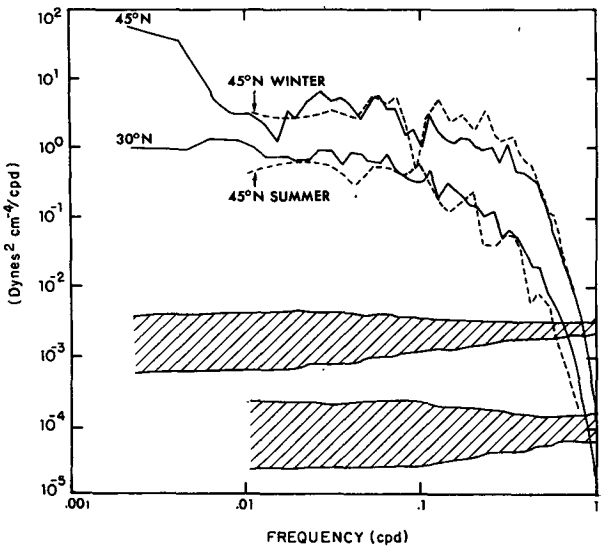

FIG. 3. The solid curves are spectra of τ^y at 30°N and 45°N (stations 4 and 3). The dotted curves are spectra of τ^y at 45°N for the winter and for the summer, each computed by averaging spectra for three successive winters or summers. The upper 95% confidence interval (shaded) applies to the full spectra and the lower 95% confidence interval applies to the seasonal spectra.

3. Analytical results

The response of an inviscid ocean to winds fluctuating at high frequencies depends on the passage of coastal-trapped waves. In the absence of continental shelf topography these waves are known as coastal Kelvin waves. Two time-scales are important: the time-scale of the forcing function and the time-scale T_k that characterizes the adjustment of the coastal zone to a change in the wind conditions. Then T_k is the time it takes a coastal Kelvin wave to travel at its free speed C across the alongshore extent of a storm of length L so that $T_k = L/C$. Upon the sudden onset of a steady meridional windstress τ^y parallel to a coast, a coastal jet develops initially ($t < T_k$). The passage of a coastal Kelvin wave excited at the boundary of the forced region establishes equilibrium conditions by introducing an alongshore pressure gradient that balances the wind stress (Allen, 1976). These results suggest that in the case of winds that fluctuate over a spectrum of frequencies, the oceanic response may be divided into frequencies greater than and less than $1/T_k$.

To determine the statistical properties of the response in these frequency ranges we turn to a model of the ocean with one active layer overlying a deep passive layer and a vertical coast. This is a reasonable model of coastal circulation in the sense that coastal currents and upwelling are observed to occur primarily in the upper ocean. The change in density between the layers, $\Delta\rho$, is assumed to be small compared to the mean density ρ. Motion of the fluid in the upper layer is described by

$$\left.\begin{aligned} U_t - fV &= \frac{-P_\theta}{a\cos\phi} + \frac{\tau^\theta}{\rho H} + F \\ V_t + fU &= -\frac{P_\theta}{a} + \frac{\tau^\phi}{\rho H} + F^\theta \\ P_t + \frac{C^2}{a}\left\{U_\theta + \frac{[\cos(\phi)V]_\phi}{\cos(\phi)}\right\} &= 0 \end{aligned}\right\}. \qquad (3.1)$$

Here U and V are the zonal and meridional velocity components corresponding to east longitude and latitude, θ and ϕ, H is the depth of the active layer, $f(\phi) = 2\Omega\sin(\phi)$ is the inertial frequency for Ω the angular speed of the earth, and $C = (gH\Delta\rho/\rho)^{1/2}$ is the speed of internal waves in the irrotational system (when $f \equiv 0$). The interface height, movement of which indicates upwelling, is $\eta = -P\rho/(\Delta\rho g)$ where P/ρ is the pressure at the height of the mean surface. Frictional terms are represented by F^θ and F^ϕ, and surface stress by τ^θ and τ^ϕ. Charney (1955) considers a similar model (although with motion possible in the lower level) on a constant f-plane. Equations (3.1) in fully spherical coordinates will be used in Section 4. Here we treat the approximate version of these equations in Cartesian coordinates.

For forcing with periods longer than a day and shorter than T_r, the period at which Rossby waves become available, for winds with no zonal variation blowing along a meridional coastline, and in the absence of friction, Gill and Clarke (1974) show that (3.1) reduces to the following two simple equations

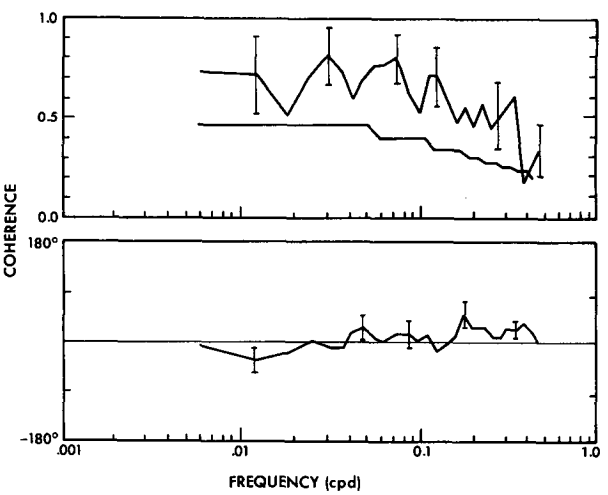

FIG. 4. Alongshore coherence amplitude and phase of τ^y at 125°W between two stations at 45 and 37°N. The phase is positive if the northern station leads the southern station. The 95% confidence limits are marked by vertical lines.

for the meridional velocity and the geostrophically related pressure near the coast:

$$V_t + CV_y = \tau(y, t), \tag{3.2a}$$

$$P = CV(y, t), \tag{3.2b}$$

where $\tau = \tau^y(y, t)/(\rho H)$. Here y is the Cartesian coordinate in the latitudinal direction, and V in this equation is the corresponding velocity component. Equation (3.2a) may be treated as a stochastic differential equation where $\tau(y, t)$ is a random variable known only in terms of its statistics.

We denote Fourier transforms by a caret. Then from (3.2a):

$$\hat{V} = \frac{\hat{\tau}(\sigma, l)}{i(Cl - \sigma)},$$

where

$$\hat{V} = \frac{1}{2\pi} \int_{-\infty}^{\infty} \int e^{-i\sigma t + ily} V(y, t)\, dt\, dy.$$

The spectrum of V is thus related to the power spectrum of the meridional wind stress, denoted $E_\tau(\sigma, l)$, by

$$E_V(\sigma, l) = \frac{\langle \hat{V}\hat{V}^* \rangle}{2\Delta l \Delta\sigma} = \frac{E_\tau(\sigma, l)}{(Cl - \sigma)^2}, \tag{3.3}$$

where angle brackets represent averages over all realizations of the spectra and the asterisk denotes complex conjugates (Müller and Frankignoul, 1981). The power spectrum as a function of frequency alone may be obtained from (3.3) by integrating over all wavenumbers:

$$E'_V(\sigma) = \int_{-\infty}^{\infty} \frac{E_\tau(\sigma, l)}{(Cl - \sigma)^2}\, dl. \tag{3.4}$$

To evaluate this integral it is necessary to know the spectrum E_τ of the wind. Consider a simplified wind field that is stationary with energy $E_0/2$ at wavenumbers $\pm l_0$. For simplicity the primes will be neglected. In this case

$$\frac{E_V(\sigma)}{E_\tau(\sigma)} = \frac{1}{2(Cl_0 - \sigma)^2} + \frac{1}{2(Cl_0 + \sigma)^2}. \tag{3.5}$$

This expression is singular at frequency $\sigma = Cl_0$, where atmospheric disturbances that travel poleward at speed C resonantly excite oceanic Kelvin waves. In reality, friction and the finite meridional extent of the ocean will limit the resonant amplification of the response at this frequency, Cl_0, which is the inverse of the time-scale T_k.

Equation (3.5) implies a change in the oceanic response at $\sigma = Cl_0$. At high frequencies, $\sigma \gg Cl_0$,

$$\frac{E_V(\sigma)}{E_\tau(\sigma)} \sim \sigma^{-2} \tag{3.6}$$

but at low frequencies, $\sigma \ll Cl_0$,

$$\frac{E_V(\sigma)}{E_\tau(\sigma)} \sim \frac{1}{(Cl_0)^2}. \tag{3.7}$$

The correlation scale of the wind has been estimated to be ~1000 km. If we assume that the wavelength is twice the correlation scale, $l_0 = 2\pi/2000$ km^{-1}, and assume that $C = 2.5$ m s^{-1}, then $Cl_0 \sim 0.1$ cpd. From results in Section 2 we know that $E_\tau \sim \sigma^{-b}$ where b has a value between 1 and 2 at high frequencies, $\sigma > Cl_0$, and b has a value less than 1 at low frequencies. It follows that at high frequencies the spectrum of the oceanic response is red,

$$E_V \sim \sigma^{-\alpha},$$

where α has values between 3 and 4 at frequencies $\sigma > Cl_0 = 0.1$ cpd. At frequencies much less than 0.1 cpd, the spectrum of the response is the same as that of the forcing and is almost white.

One of the effects of friction on the spectra may be determined by introducing a linear friction term, $-RV$, into the left-hand side of (3.2a). A similar friction parameterization has been suggested by Brink and Allen (1978) for barotropic coastal dynamics in the presence of a weak bottom Ekman layer. When $R \ll Cl_0$ Eqs. (3.6) and (3.7) are unchanged but when $R \gg Cl_0$, at low frequencies $E_V(\sigma)/E_\tau(\sigma) \sim R^{-2}$. Friction controls the strength of the current. In this paper we are mainly interested in the circulation when the friction is weak.

The cross-spectra between oceanic and meteorological variables at the same location, and between oceanic variables separated in space, also change at the frequency Cl_0. The coherence between random variables $Y(\sigma, l)$ and $X(\sigma, l)$, linearly related by $Y(\sigma, l) = T(\sigma, l)X(\sigma, l)$, when integrated over all wavenumbers, is

$$\mathrm{Coh}_{YX}(\sigma) = \frac{S_{YX}(\sigma)}{[E_X(\sigma)E_Y(\sigma)]^{1/2}}, \tag{3.8}$$

where

$$S_{YX}(\sigma) = \int_{-\infty}^{\infty} T(\sigma, l)E_X(\sigma, l)\, dl.$$

The function $S_{YX}(\sigma)$ is the cross spectrum and $T(\sigma, l)$ is the transfer function between $X(\sigma, l)$ and $Y(\sigma, l)$. If $T(\sigma, l)$ is independent of l the coherence amplitude will be unity. Otherwise destructive interference will reduce the coherence. For wind stress τ and alongshore current V,

$$\left.\begin{aligned} \mathrm{Coh}_{\tau V}(\sigma) &= \frac{S_{\tau V}(\sigma)}{[E_V(\sigma)E_\tau(\sigma)]^{1/2}} \\ S_{\tau V}(\sigma) &= -\int_{-\infty}^{\infty} \frac{E_\tau(\sigma, l)}{i(Cl - \sigma)}\, dl \end{aligned}\right\}. \tag{3.9}$$

If we again assume that the wind fluctuations are stationary with energy $E_0/2$ at wavenumbers $\pm l_0$, then

$$\mathrm{Coh}_{\tau V}(\sigma) = \frac{i/(Cl_0 - \sigma) - i/(Cl_0 + \sigma)}{[2/(Cl_0 - \sigma)^2 + 2/(Cl_0 + \sigma)^2]^{1/2}}. \quad (3.10)$$

At high frequencies $\sigma \gg Cl_0$ the coherence amplitude is unity and the alongshore velocity lags the wind by 90°. This reflects the unimportance of the alongshore pressure gradient in Eq. (3.1b). At low frequency $\sigma < Cl_0$ the coherence amplitude in (3.10) approaches zero.

It can readily be shown that the coherence between τ^y and the alongshore pressure gradient is

$$\mathrm{Coh}_{\tau P_y}(\sigma) = \frac{1/(Cl_0 - \sigma) + 1/(Cl_0 + \sigma)}{[2/(Cl_0 - \sigma)^2 + 2/(Cl + \sigma)^2]^{1/2}}. \quad (3.11)$$

At high frequencies the coherence, $\tau^y - P_y$, is small and is 180° out of phase with the wind stress. The pressure gradient is unimportant in the balance of forces at these frequencies. At frequencies somewhat greater than Cl_0 the coherence amplitude increases. At frequencies less than Cl_0 the coherence amplitude is unity and the phase lag is zero, reflecting a low-frequency balance between τ^y and P_y.

The coherence for two stations separated by an alongshore distance Δy is

$$\mathrm{Coh}_{V_1V_2}(\sigma) = \frac{e^{i\Delta y l_0}(Cl_0 + \sigma)^2 + e^{-i\Delta y l_0}(Cl_0 - \sigma)^2}{(Cl_0 + \sigma)^2 + (Cl_0 - \sigma)^2}. \quad (3.12)$$

The coherence amplitude is $\cos(l_0\Delta y)$ at high and low frequencies but approaches unity near $\sigma = Cl_0$. The fact that the coherence does not decay for large separation distances is a result of the artificial nature of the forcing. The phase is small at high and low frequencies. However, at frequencies near Cl_0 the poleward station lags the equatorward station by $(360\Delta y l_0/2\pi)$ degrees, since near this frequency variations in the alongshore velocity field propagate poleward at speed C.

In summary these results show that at high frequencies $\sigma > Cl_0$, the spectrum of the oceanic response is quite red, the coherence between alongshore currents and winds is high with the currents lagging by 90°, and the coherence between the alongshore wind and alongshore pressure gradient is low. At low frequencies, $\sigma < Cl_0$, the spectrum is much less red and becomes white at very low frequencies. Winds and currents are uncorrelated, but the alongshore pressure gradient is correlated with the alongshore wind.

These results depend on a number of simplifying assumptions some of which are relaxed in the next section.

4. Numerical reduced-gravity model

The analysis of Section 3 assumes that the ocean is meridionally unbounded, that the forcing is stationary in time and homogeneous in space (examine Fig. 3), and that the Coriolis parameter f is constant. To relax these assumptions we turn to a numerical model forced with the realistic winds described in Section 2. Motion is again described by (3.1), retaining the spherical coordinates, the dependence of f on latitude and wind curl. For the calculations to be described next, $C = 2.5$ m s^{-1} and H, the depth of the active upper layer, is 107 m. The model domain extends from 142 to 125°W and 23.5 to 50°N. This area is outlined in Fig. 1a.

The model contains diffusive friction of the form $F^\theta = A\nabla^2 U$, $F^\phi = A\nabla^2 V$, where $A = 2 \times 10^6$ cm^2 s^{-1}. A rough estimate of the frictional damping time of the coastal currents may be obtained by the time scale in (3.1) for which the dissipation terms balance the acceleration terms. Estimating the offshore scale of the currents as the radius of deformation, C/f, the damping time is $C^2/(Af^2) \approx 40$ days and the alongshore scale of the damping is $C^3/(Af^2) \approx 8000$ km, more than twice as long as the entire eastern boundary of the model.

The northern, southern and western boundaries have high-friction-damping layers ($A = 2.5 \times 10^8$ cm^2 s^{-1} in the south and west) to eliminate poleward and westward waves propagating away from the eastern boundary. The boundary condition requires the velocity to be zero along all four walls. The numerical resolution near the eastern coast is 0.055° in the zonal direction and 0.5° in the meridional direction. The resolution decreases towards the west. More details, including the differencing scheme used in the model, are given by Carton (1983). The wind for each time step ($\Delta T = 10$ min) is computed by linear interpolation between successive twelve hourly analyses.

Before discussing the model statistics we consider two 30-day time series, shown in Fig. 5, taken at station 3 (45°N, 125.22°W) near the eastern boundary (the position of the stations is shown in Fig. 1a). The time series have been smoothed with a 3.3-day symmetric cosine filter. The first record shows two wind events forcing offshore drift. The intensifying wind accelerates the alongshore current southward. The flow stops accelerating as an alongshore pressure gradient develops. As the wind stress weakens, the alongshore velocity and upwelling decay.

An event appears in the alongshore current which is not correlated with the wind stress in the second time series. The event must be a Kelvin wave since that is the only wave available in this system at periods of a few days. Figure 6 shows a time–latitude plot of the meridional velocity. The solid line is the

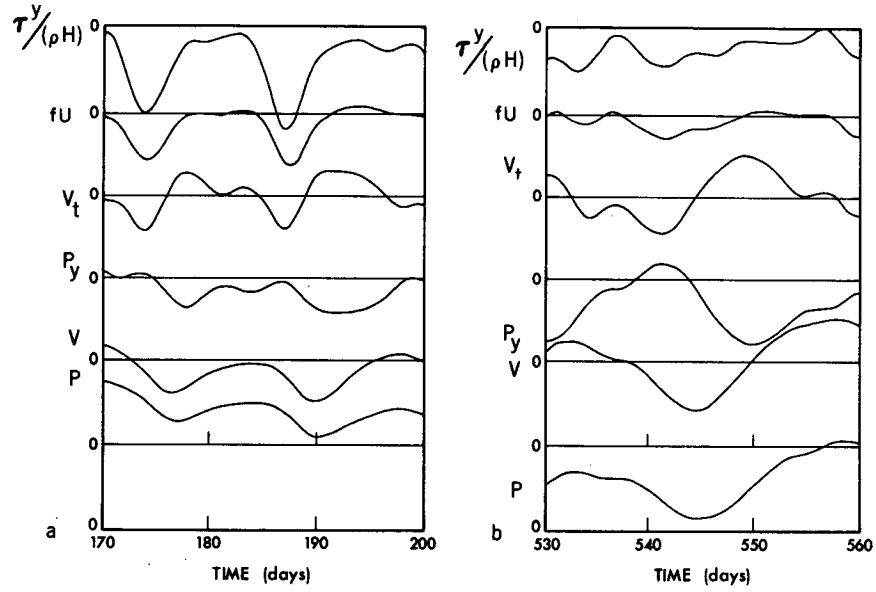

FIG. 5. Two thirty-day time series of meridional wind stress and ocean variables. The ocean data were generated by a reduced-gravity numerical model in the domain marked in Fig. 1a. All the data were collected near the eastern ocean boundary at 45°N (station 3 in Fig. 1a). The zonal and meridional velocities are U and V. The pressure at the mean surface is P. Terms are normalized so that $V_t + fU = -P_y + \tau^y/(\rho H)$ + friction. The time axis is marked in days since 31 December 1973. (a) The southward wind events cause offshore drift, southward events in the meridional velocity and pressure gradient. (b) A strong event occurs in the meridional velocity and pressure gradient which is not associated with the local wind stress.

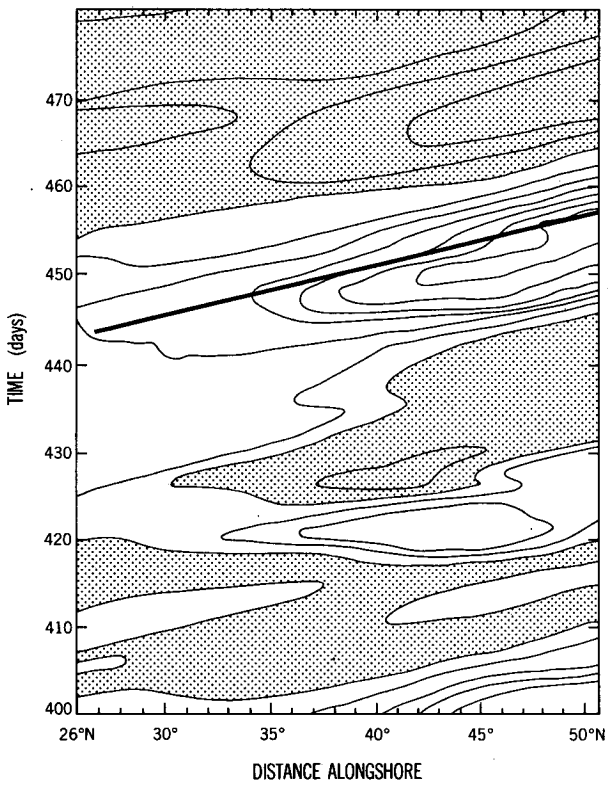

FIG. 6. Alongshore vs time cross section of V at 125°W. A line of constant phase for Kelvin waves is marked with a solid line. The contour interval is 1 cm s^{-1}. Shaded regions are negative.

line of propagation of a free Kelvin wave. While still growing, these waves travel somewhat faster than the free-wave speed. This is an interference effect between a wind-driven jet and the free wave it generates (Gill and Schumann, 1974; Chao, 1981; Philander and Yoon, 1982). A superposition of many such free and forced events comprises the statistics of the ocean response.

Figures 5 and 6 illustrate the role of coastal Kelvin waves. In addition to these waves, Rossby waves are possible because the latitudinal gradient of the Coriolis parameter is taken into account. These waves come into play after a time $T_r = 4\pi f/(\beta C)$ when the coastal jet starts to disperse westward into Rossby waves (Anderson and Gill, 1975; McCreary, 1977; Philander and Yoon, 1982). On time-scales long compared to T_r the oceanic response is a Sverdrup balance, and the offshore scale is no longer the radius of deformation but is the distance Rossby waves travel in a given time.

Ocean statistics. The rms alongshore ocean velocity, as high-pass ($T \leq 33$ days), low-pass ($T \geq 33$ days), and a very-low-pass filtered ($T \geq 110$ days), is given in Figs. 7a, b and c. In Fig. 7a a distinctive narrow coastal current is evident although there is no intensification in the wind near the coast. Its width is approximately the scale of the radius of deformation, $C/f \sim 25$ km. At longer periods (Figs. 7b, c) the flow disperses westward, as predicted earlier (in midlatitudes $T_r \approx 300$ days).

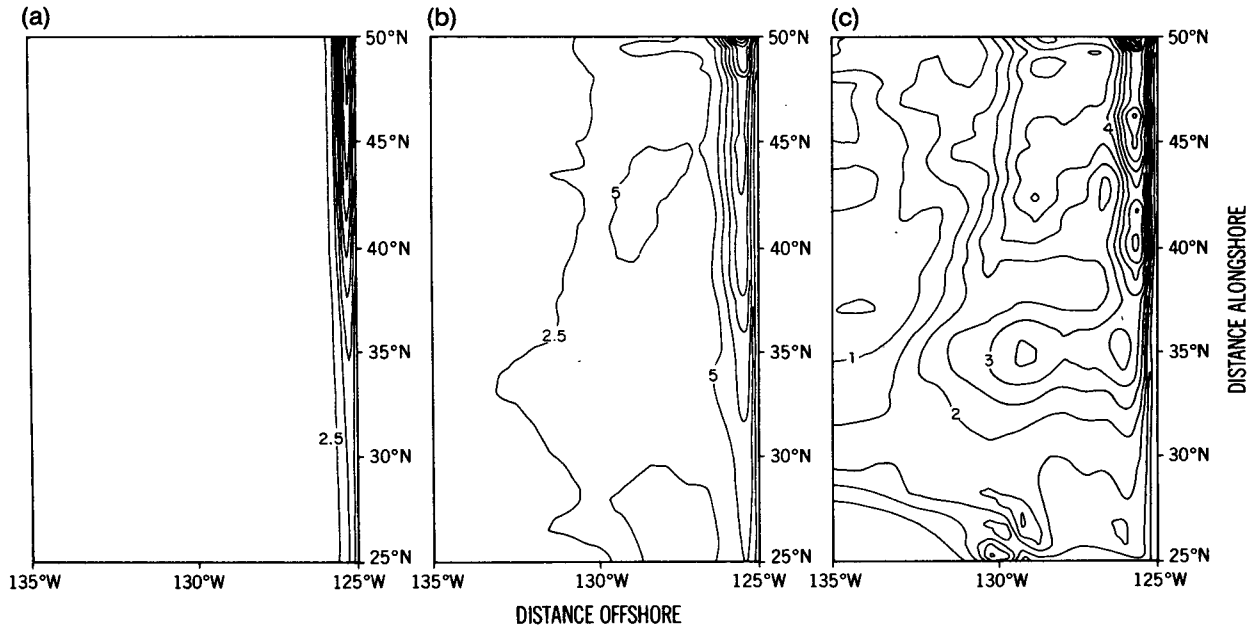

FIG. 7. Zonal–meridional plot of rms V. (a) High-pass filtered ($t < 33$ d), (b) low-pass filtered ($t > 33$ d), (c) very low-pass filtered ($t > 110$ d). Contour intervals are 2.5 cm s^{-1}, 2.5 cm s^{-1}, and 0.5 cm s^{-1}. As the period decreases the current spreads westward.

Variability of the current increases poleward both because the wind is stronger there and because disturbances in the flow propagate poleward and so have a cumulative effect. In Fig. 7c there is an indication of a peak at 45°N, corresponding to a peak in the intensity of the alongshore winds. There is also a suggestion of a larger offshore scale at lower latitudes. This can be attributed to the higher speed of Rossby waves in low latitudes.

Spectra. Spectra for data from the four stations indicated in Fig. 1a have been computed in the same way as the wind spectra. Station 1 is nearshore at 42.5°N, station 2 is 1.2° offshore at 45°N, station 3 is nearshore at 45°N, and station 4, nearshore at 30°N. Subscripts (1, 2, 3, 4) of various quantities refer to the station at which the quantities are measured. We present the normalized spectra of V, P, and P_y in Fig. 8, all computed at station 3. The spectra are normalized with respect to the spectrum of the meridional wind stress at station 3. This was done in order to emphasize the behavior of these spectra which is due to dynamics rather than to the shape of the forcing. The confidence intervals shown are those estimated for the individual spectra.

At frequencies between 0.1 and 0.5 cpd, $E_{V3}(\sigma)/E_{\tau 3}(\sigma)$ behaves as $\sim\sigma^{-3}$, more red than expected from (3.6). At lower frequencies the slope is σ^{-2} until 0.01 cpd approximately. At still lower frequencies the spectrum appears to decay. It is striking that whereas analysis based on (3.3) led us to anticipate a change in the slope of E_V/E_τ at a period of 10 days, no change is evident at that period in the solid line in Fig. 8. The value of 10 days is an estimate for $1/(Cl_0)$, the time it takes a Kelvin wave to propagate a distance $1/l_0$. In the analytical model of Section 3 we assumed that the energy of the wind is concentrated at meridional wavenumbers $\pm l_0$. In reality, the wind has energy over a broad band of meridional wavenumbers and is inhomogeneous in alongshore distribution. Because of these factors there is no precise frequency Cl_0 at which the oceanic response changes

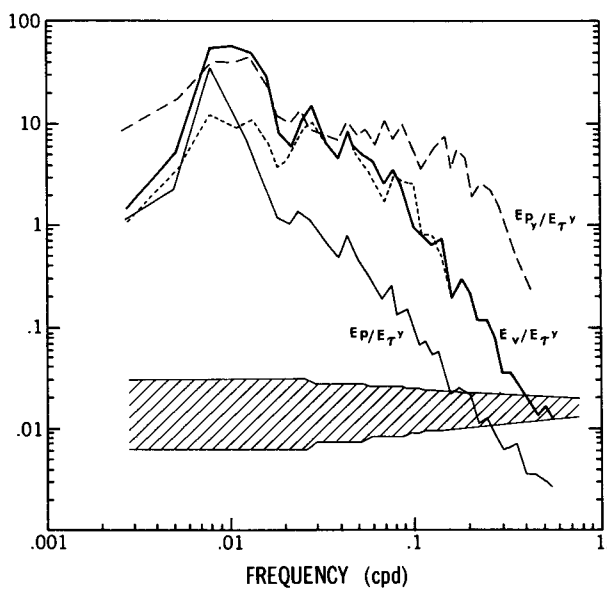

FIG. 8. Normalized alongshore velocity spectrum $E_V(\sigma, y_3)/E_\tau(\sigma, y_3)$, normalized pressure spectrum $E_P(\sigma, y_3)/E_\tau(\sigma, y_3)$, and pressure-gradient spectrum $E_{Py}(\sigma, y_3)/E_\tau(\sigma, y_3)$. The short dashed curve is $E_V(\sigma, y_3)/E_\tau(\sigma, y_3)$ for model run without wind stress curl (see text for discusson). The units of the ordinate are arbitrary.

abruptly, but rather a band of frequencies in which the response changes gradually.

Figure 8 shows that much of the variability is at relatively long periods—up to (approximately) 100 days. Similarly, Bryden's (1978) calculations of vertical velocity off Oregon showed as much variability at monthly periods as at daily periods. Some of this variability is associated with forcing by the curl of the wind stress, a factor neglected in Section 4. To quantify the effect of the curl, we reran the model with a wind field defined by $\tau = [0, \tau^{\phi}(\theta = 125°\text{W}, \phi)]$, which has no curl but retains the same alongshore component of the wind stress as the original wind stress field. The short dashed curve in Fig. 8 shows the spectrum of V generated by the filtered wind. The spectrum now has a distinctive flattening at periods longer than 50 days or so. The difference in the two spectra between 50- and 200-day periods suggests that at these periods, curl in the wind stress is important. At longer periods the alongshore velocity spectrum decays as the offshore scale increases on account of the β-effect.

The ratio of the spectrum of P_y to the spectrum of τ^y, $E_{Py3}(\sigma)/E_{\tau 3}(\sigma)$, is white even at high frequencies ($\sigma \leq 0.33$ cpd). High wavenumbers are given extra weight in determining $E_{Py3}(\sigma)$ because P_y is proportional to the alongshore derivative of V at high frequency, from (3.2b). For that reason the frequency at which the spectrum shifts from red to white is higher for $E_{Py3}(\sigma)$ than for $E_{V3}(\sigma)$. This result was not anticipated by our example with the analytical model because in that example we considered forcing that is sinusoidal in distance alongshore. With that forcing, taking alongshore derivatives does not increase the "roughness" of the forcing.

The ratio $E_{P3}(\sigma)/E_{Py3}(\sigma)$ gives a measure of the dominant alongshore length scale of the pressure as a function of frequency. For frequencies less than 0.03 cpd the frequency-averaged length scale is 1230 km which is essentially that of the forcing. For frequencies between 0.03 and 0.5 cpd the length scale drops to 365 km, smaller than the scale of the wind stress. This indicates that at high frequencies the scale of the response is determined by dynamics rather than by the scale of the forcing (short Kelvin waves are excited at high frequencies). The difference between low and high frequencies is further confirmation that pressure gradients balance the wind stress at low frequencies.

Coherence. The coherence between wind stress and model variables at 45°N, 125.22°W is shown in Fig. 9. The coherences have been computed from the four-year record, cut into 15 overlapping 175-day segments, but otherwise treated as when computing the spectra. The shorter segment lengths were chosen in order to increase the confidence of the coherence estimates. The zonal velocity is coherent with the wind stress with no phase lag at frequencies above

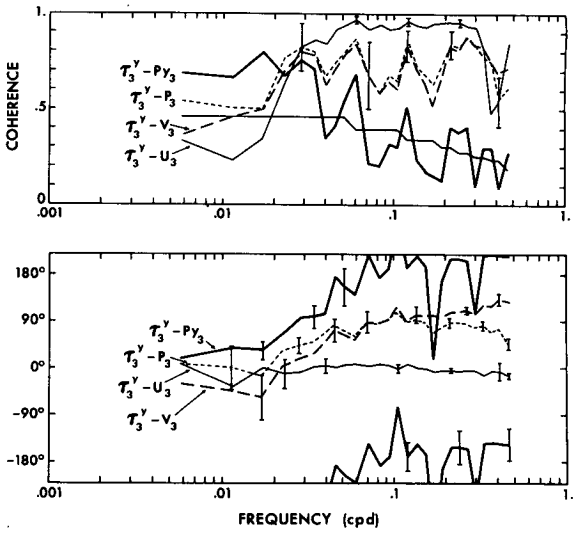

FIG. 9. Coherence amplitude and phase between $\tau_3^y - U_3$, $\tau_3^y - V_3$, $\tau_3^y - P_3$, and $\tau_3^y - P_{y3}$. The phase is positive if the first variable leads the second variable. The 95% confidence limits are marked with vertical lines.

0.02 cpd. This is consistent with Ekman drift in which a southward wind causes offshore flow in the surface layer. At lower frequencies the coherence decreases as the wind-stress curl becomes important.

The meridional velocity nearshore has high coherence with τ^y down to a frequency of 0.02 cpd approximately. The meridional velocity lags τ^y by 90° at high frequencies, consistent with the analytical model. The coherence decays gradually as the frequency decreases below $1/T_k$. At these low frequencies the $\tau^y - P_y$ coherence increases as the alongshore pressure gradient comes into balance with the alongshore wind stress.

Two-point coherences have been computed between time series sampled at stations 1, 2, and 3 (Fig. 10). The zonal velocity is relatively incoherent in the alongshore direction (not shown) but is highly coherent in the offshore direction. Both P and V are highly coherent alongshore. The observed phase lag of P_y between two points separated alongshore is consistent with the alongshore speed of free Kelvin waves of 2.5 m s^{-1}. The alongshore velocity field shows a reduced lag at high frequencies.

Seasonal response of the reduced-gravity ocean. Within 1000 km of the coastal upwelling zones of Washington, Oregon, and California lies the California Current System. This current system has both southward and northward flowing branches, each with a width ~ 200 km. Hickey (1979) shows that the mean alongshore velocity and seasonal variation of the alongshore velocity in these branches are each 5–10 cm s^{-1}. Other measurements discussed by White and Saur (1982) show westward propagation of waves farther out in the eastern North Pacific. These waves

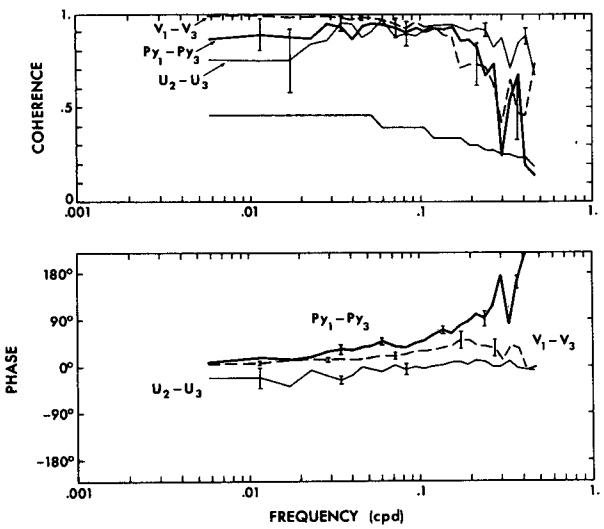

FIG. 10. Coherence amplitude and phase between $U_2 - U_3$, $V_1 - V_3$, and $P_{y1} - P_{y3}$. The phase is positive if the first variable leads the second variable. The 95% confidence limits are marked with vertical lines.

have periods of one to two years and appear to originate near the eastern boundary. How is the coastal circulation connected to the seasonal circulation in the interior ocean? In this section we address this question by examining the seasonal response of the reduced-gravity ocean.

At high frequencies upwelling and alongshore currents are confined near the coastline. As the frequency decreases toward $1/T_r$ the ocean dynamics change and alongshore currents begin to spread westward away from the coast. Figure 11a shows a "snapshot" view of the meridional velocity field at day 350, after the data have been low-pass filtered with a 110-day bandwidth filter. Alternating alongshore currents are visible near the coast with the offshore scale of zonally traveling Rossby waves at annual periods. The scale of the currents increases at low latitudes as does the Rossby wavelength. The alongshore currents are 5 cm s^{-1}, comparable to observed velocities. The intensity of the alongshore currents, however, depends on the parameters C and H.

At seasonal frequencies two components of the wind field have been considered as possibly driving the seasonal circulation of the eastern ocean. Bryan and Ripa (1978), Hickey (1979), Chelton (1984), and others have suggested that upwelling due to curl of the wind stress is important in setting up pressure gradients. In Section 4 we verified that wind stress curl was important at periods longer than 50 days. The work of Anderson and Gill (1975) and Philander and Yoon (1982) suggests that the alongshore component of the wind stress, which need not contain any curl, can also contribute to the seasonal variability of the California Current system because of the presence of a strong annual signal in the alongshore wind stress.

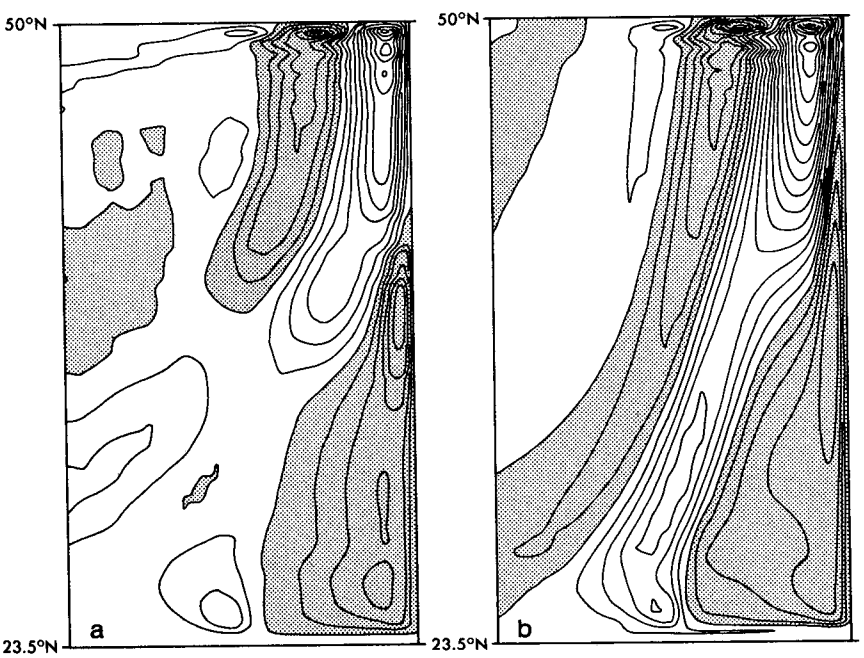

FIG. 11. Zonal–meridional plot of meridional velocity low-pass filtered (B_w = 110 d) at day 350. (a) Model with complete wind field, and (b) model run with no $\nabla_h \times \tau$ (see text for discussion). The plots extend zonally from 135.6 to 125.22°W (at 45°N the plots are 815 km wide). Contour intervals are 2.5 and 1.0 cm s^{-1}. Shaded regions are southward flowing.

The relative importance of these two mechanisms can be estimated by comparing the response to the actual winds with the response to winds without curl (in the latter case the alongshore winds at the coast are assumed to prevail everywhere). It is found that the flow within 300 km of the coast is primarily determined by the alongshore winds and has the structure shown in Fig. 11b. Farther offshore where the intensity of the wind increases (see Fig. 1) the curl of the wind is probably the dominant mechanism for driving currents.

5. Discussion

Previous studies of wind-driven coastal circulation have shown that the strength of coastal currents and intensity of upwelling depend not only on the strength of the wind but also on the width of the storms, the duration of the storms and any alongshore movement of the storms. In particular, studies of the inviscid ocean suggest that the oceanic response may be characterized by three frequency ranges: $\sigma < 1/T_k$, $1/T_r < \sigma < 1/T_k$, and $\sigma < 1/T_r$. In these inviscid studies T_k is the time a Kelvin wave takes to establish an alongshore pressure gradient in the coastal zone after a change in wind conditions, and T_r is the time-scale on which Rossby wave dispersion becomes important.

Description of the wind field in this study suggests that $1/T_k$ is of the order of 0.1 cpd. At higher frequencies the spectrum of the response increases sharply with decreasing frequency ($\sim\sigma^{-3}$), the alongshore current is highly correlated with the alongshore wind (and lags by 90°) but the alongshore pressure gradient is not correlated with the alongshore wind. At low frequencies $\sigma < 1/T_k$ the spectrum of current is much less red, correlation between the alongshore current and wind is low but it is high for the alongshore pressure gradient and the wind.

Results from a reduced-gravity model forced with realistic winds indicate that the transition from the high-frequency to low-frequency response takes place gradually over a broad band of frequencies from 0.1 to 0.02 cpd approximately. This happens because there is no single length scale that characterizes the surface winds which furthermore are spatially inhomogeneous. At frequencies below 0.02 cpd the curl of the wind contributes significantly to the variability near the coast, and is dominant at distances more than 300 km from the coast. These two results depend on the choice of the free parameter $C = (gH\Delta\rho/\rho)^{1/2}$. As the stratification increases, the frequency at which the wind stress curl becomes important also increases.

These results are in reasonable agreement with measurements. Cutchin and Smith (1973), Huyer *et al.* (1975), and Kundu and Allen (1976) find that the spectra of observed alongshore currents off the coast of Oregon are red, behaving as σ^{-3} at frequencies above 0.15 cpd. At frequencies less than 0.15 cpd the spectra appear to flatten out but the short record lengths make this conclusion tentative.

Huyer *et al.* (1975) and Huyer and Smith (1978) show correlations between the northward component of the wind (approximately alongshore) and the alongshore current range from 0.4 to 0.7. Smith (personal communication, 1982) analyzed a year-long record and found coherences of $\tau^y - V$ of 0.6 at high frequency with the velocity lagging behind the wind. At the seasonal time-scale Hickey and Pola (1983) find that alongshore pressure gradients and alongshore winds are highly correlated. Chelton (1984) has argued, based on an analysis of geostrophic wind and current data, that the curl of the wind is an important forcing function on these long time-scales.

The reduced-gravity model that has been used in these studies is incapable of resolving the observed vertical structure of the flow—there is no coastal undercurrent for example. The reduced-gravity model is also flawed in that it is associated with a single gravity-wave speed C whereas a continuously stratified ocean has a spectrum of speeds. The inclusion of bottom topography modifies the structure of coastal waves, introduces bottom friction and a topographic β-effect. A multi-level numerical model will be necessary to investigate how these factors affect the statistics of the oceanic response to realistic winds.

Acknowledgment. The authors thank the members of the Geophysical Fluid Dynamic Laboratory for encouraging this work. G. Mellor, K. Bryan and K. Brink provided many useful comments on this manuscript. Drafting help was provided by P. Tunison and his staff. Typing was done by R. D'Arcangelo. One of the authors (JAC) was supported by NSF Grant ATM9106800, and also by Harvard University under ONR Grant N00014-75-C-0225.

REFERENCES

Allen, J. S., 1976: Some aspects of the forced wave response of stratified coastal regions. *J. Phys. Oceanogr.*, **6**, 113–119.

Anderson, D. L. T., and A. E. Gill, 1975: Spin-up of a stratified ocean, with applications to upwelling. *Deep-Sea Res.*, **22**, 583–596.

Bakun, A., 1975: Daily and weekly upwelling indices, West Coast of North America 1967–1973. NOAA Tech. Rep. NMFS SSRF-693, 114 pp.

Bloomfield, P. B., 1976: *Fourier Analysis of Time Series: An Introduction.* Wiley and Sons, 258 pp.

Brink, K. H., and J. S. Allen, 1978: On the effect of bottom friction on barotropic motion over the continental shelf. *J. Phys. Oceanogr.*, **8**, 920–922.

Bryan, K., and P. Ripa, 1978: The vertical structure of North Pacific temperature anomalies. *J. Geophys. Res.*, **83**, 2419–2429.

Bryden, H., 1978: Mean upwelling velocities on the Oregon continental shelf during summer 1973. *Estuaries Coastal Mar. Sci.*, **7**, 311–327.

Carton, J. A., 1983: Adjustment in the oceans: The long-period tides and coastal upwelling. Ph.D. dissertation, Princeton University, 212 pp.

——, 1984: Coastal circulation caused by an isolated storm. *J. Phys. Oceanogr.*, **14**, 114–124.

Chao, S.-Y., 1981: Forced shelf circulation by an alongshore wind band. *J. Phys. Oceanogr.*, **11**, 1325–1333.

Charney, J. G., 1955: The generation of oceanic currents by wind. *J. Mar. Res.*, **14**, 477–498.

Chelton, D. B., 1984: Seasonal variability of alongshore geostrophic velocity off central California. *J. Geophys. Res.*, **89**, 3473–3486.

Cutchin, D. L., and R. L. Smith, 1973: Continental shelf waves: Low frequency variations in sea level and currents over the Oregon continental shelf. *J. Phys. Oceanogr.*, **3**, 73–83.

Gill, A. E., and A. J. Clarke, 1974: Wind-induced upwelling, coastal currents and sea-level changes. *Deep-Sea Res.*, **21**, 324–345.

——, and E. H. Schumann, 1974: The generation of long shelf waves by the wind. *J. Phys. Oceanogr.*, **4**, 83–90.

Hickey, B. M., 1979: The California Current System—hypotheses and facts. *Progress in Oceanography*, Vol. 8, Pergamon, 191–279.

——, and N. Pola, 1983: The alongshore pressure gradient on the west coast of the United States. *J. Geophys. Res.*, **86**, 7623–7633.

Huyer, A., and R. L. Smith, 1978: Seasonal differences in low-frequency current fluctuations over the Oregon continental shelf. *J. Geophys. Res.*, **83**, 5077–5089.

——, B. M. Hickey, J. D. Smith, R. L. Smith and R. D. Pillsbury, 1975: Alongshore coherence at low frequencies in currents observed over the continental shelf off Oregon and Washington. *J. Geophys. Res.*, **80**, 3495–3505.

Kundu, P. K., and J. S. Allen, 1976: Some three-dimensional characteristics of low-frequency current fluctuations near the Oregon coast. *J. Phys. Oceanogr.*, **6**, 181–199.

McCreary, J. P., 1977: Eastern ocean response to changing wind systems. Ph.D. thesis, University of California at San Diego, 156 pp.

Müller, P., and C. Frankignoul, 1981: Direct atmospheric forcing of geostrophic eddies. *J. Phys. Oceanogr.*, **11**, 287–308.

Nelson, C. S., 1977: Wind stress and wind stress curl over the California Current. NOAA Tech. Rep. NMFS SSRF-714, U.S. Dept. of Commerce, 89 pp.

Philander, S. G. H., and J.-H. Yoon, 1982: Eastern boundary currents and coastal upwelling. *J. Phys. Oceanogr.*, **12**, 862–879.

Suginohara, N., 1982: Coastal upwelling: Onshore-offshore circulation, equatorward coastal jet and poleward undercurrent over a continental shelf-slope. *J. Phys. Oceanogr.*, **12**, 272–284.

White, W. B., and J. F. T. Saur, 1982: A source of annual baroclinic waves in the eastern subtropical North Pacific. *J. Phys. Oceanogr.*, **11**, 1452–1462.

Willebrand, J., 1978: Temporal and spatial scales of the wind field over North Pacific and North Atlantic. *J. Phys. Oceanogr.*, **8**, 1080–1094.

Yoshida, K., 1955: Coastal upwelling off the California coast. *Rec. Oceanogr. Works Japan*, **15**, 1–13.